# Optical Isolation with Optical Parametric Amplification in an Atomic System

*Changbiao Li, Qingsong Yu, Yanpeng Zhang, Min Xiao, and Zhaoyang Zhang\**

**Magnet-free active optical nonreciprocal (AON) devices free from insertion loss help to establish optical information processing networks involving weak signals without introducing external magnetic fields. However, considering the necessary resonant condition for amplification or the presence of optical resonators for most demonstrated magnet-free AON schemes, it remains a challenge to broaden the AON bandwidth. Here the optical isolation based on optical parametric amplification is demonstrated experimentally in a coherent three-level atomic configuration. With the phase-matching condition satisfied or not by oppositely launching the probe beams, they can pass through the medium experiencing parametric amplification or strong resonant absorption. Such magnet- and cavity-free optical isolation exhibits a maximum isolation ratio of 46.5 dB and a broad bandwidth of over 0.85 GHz for the isolation ratio ≥30 dB. The demonstrated results arising from atomic-coherence-based optical parametric process with quantum nature pave the way to achieve high-performance nonreciprocal quantum information processing.**

## 1. Introduction

Optical nonreciprocity associated with breaking the time-reversal symmetry for light propagation can act as the counterpart of unidirectional transmission widely applied in electronic circuits, thus offers promising opportunities for the development of desired functionalities such as optical isolation and circulation indispensable for both classical and quantum optical signal processing.[1,2] During recent years, the discoveries of various approaches for optical nonreciprocity, such as spatiotemporal

C. Li, Q. Yu, Y. Zhang, Z. Zhang
Key Laboratory for Physical Electronics and Devices of the Ministry of Education & Shaanxi Key Lab of Information Photonic Technique, School of Electronic Science and Engineering, Faculty of Electronic and Information Engineering
Xi'an Jiaotong University
Xi'an, Shaanxi 710049, China
E-mail: zhyzhang@xjtu.edu.cn
M. Xiao
Department of Physics
University of Arkansas
Fayetteville, Arkansas 72701, USA
M. Xiao
National Laboratory of Solid State Microstructures and School of Physics
Nanjing University
Nanjing, Jiangsu 210093, China

modulation,[3–5] optical nonlinearity,[6–9] aluminum nitride piezoelectric modulation,[10] Autler-Townes splitting,[11] and even energy loss,[12] have allowed the nonreciprocal optical devices to become capable of being effectively integrated with optical signal processing networks by avoiding the bulky magnets and crosstalk of external magnetic fields, which are needed in traditional magneto-optical Faraday effect.[13] To date, such magnet-free optical nonreciprocity has been realized in a variety of optical platforms including cavity optomechanical systems,[14–16] photonic waveguides,[17] atomic gases[18–25] and metasurfaces,[26] among others, with individual physical mechanism to bypass the Lorentz reciprocity theorem. In particular, considering the advancement in realizing the miniaturization and integration of atomic samples,[27,28] multilevel atomic systems with readily manipulated light-induced atomic coherence have spawned flourishing achievements in optical nonreciprocity by taking advantages of inherent atomic properties such as the thermal-motion induced Doppler shift[18–20] and the transition rules between energy levels.[29] Strikingly, the recently reported collision-induced optical nonreciprocity in an atomic configuration driven by three laser fields has reached the maximum isolation ratio of ≈40 dB with the insertion loss ≤1 dB and a bandwidth of ≈200 MHz for isolation ratio ≥30 dB.[21] Also, a high-performance optical isolation in single-photon level was realized via electromagnetically induced transparency in an atomic vapor cell.[20]

Among the functionalities arising from optical nonreciprocity, active nonreciprocal components free from insertion loss, such as nonreciprocal amplification, possess distinct features in measuring weak signals and protecting the signal source from disturbance of excess noises in communication and signal processing.[30] Optical nonreciprocal amplification has been demonstrated based on non-Hermitian properties,[31,32] resonantly enhanced Brillouin interaction,[33] chiral stimulated Raman scattering,[34] reservoir engineering,[35] optical parametric process,[36] and atomic-coherence-induced Raman gain,[17] to name a few. Despite the exciting progresses in this area, most experimental realizations of nonreciprocal amplification exhibit a limited bandwidth due to the resonant condition necessary for amplification or the narrow-bandwidth feature of the adopted elements for constructing the nonreciprocal systems. Schemes
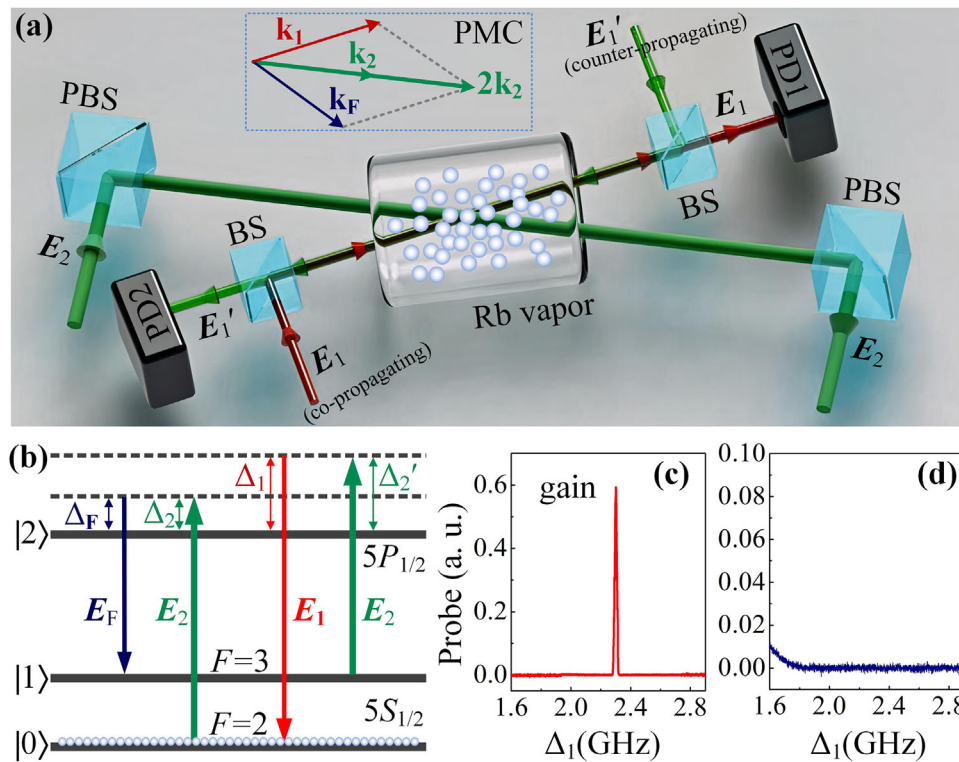
**Figure 1.** a) Experimental setup. The weak probe beam $E_1$ nearly copropagating with the strong pump beam $E_2$ experiences optical parametric amplification, while the other probe $E_1'$ (travelling in opposite direction with $E_1$) exhibits strong Doppler absorption. Probe beams are derived from a continuous-wave single-mode tunable external cavity diode laser (ECDL) with a wavelength of ≈795 nm. The pump field $E_2$ is the output of a semiconductor tapered laser amplifier seeded with a laser from the other continuous-wave ECDL (≈795 nm). The angle between $E_1$ and $E_2$ is ≈0.2°. The temperature of the 5 cm long rubidium vapor cell is set to 120 °C by a heating tape. The inset (marked by a dashed box) shows the phase-matching condition ($\mathbf{k}_1 + \mathbf{k}_F = 2\mathbf{k}_2$) for optical parametric amplification. PD1 and PD2 represent two branches of a balanced homodyne detector. PBS: polarization beam splitter; BS: 50/50 beam splitter; PD: photodiode. b) The double-Λ energy-level structure coupled by the pump and the probe beams. (c) and (d) show the observed transmission spectra of the co- and counter-propagating probe fields, respectively. Both probe beams are simultaneously present for the experimental measurements.

for high-performance nonreciprocal amplifier with both high isolation ratio and broad bandwidth remain to be further explored.

In this article, by taking advantage of the multiparameter tunable optical parametric amplification requiring phase-matching condition (PMC) in an atomic vapor cell, we experimentally demonstrate the optical nonreciprocal amplification as well as high-performance optical isolation with a high isolation ratio and broad bandwidth in a coherently prepared three-level double-Λ atomic configuration. With the incident weak probe beam arranged to copropagate with the strong pump beam in a small angle to meet the PMC, the output probe beam can experience parametric amplification with a high gain factor. However, if the probe beam is launched along the opposite direction, it will suffer strong Doppler absorption and have no gain due to the lack of proper phase matching. As a consequence, the isolation ratio reaches as high as 46.5 dB with both probe beams (launched in opposite directions) switched on, and the bandwidth for isolation ratio exceeding 30 dB gets over 0.85 GHz. Moreover, this double-Λ atomic configuration is also employed to effectively produce entangled photon pairs and squeezing states,[37,38] and the demonstrated cavity-free and magnet-free optical isolation may find promising applications in quantum networks.

## 2. Experimental Scheme

The schematic experimental setup is depicted in **Figure 1**a, in which the weak probe beam $E_1$ and pump beam $E_2$ propagate along almost the same direction and intersect inside the vapor cell with a small angle to drive the three-level double-Λ atomic configuration shown in Figure 1b. The weak beam $E_1$ (frequency $\omega_1$, wavevector $\mathbf{k}_1$, Rabi frequency $\Omega_1$, horizontal polarization) couples the transition between the excited state $5P_{1/2}$ (level $|2\rangle$) and a hyperfine state $F = 2$ ($|0\rangle$) of the ground state $5S_{1/2}$ of $^{85}$Rb atoms, while the strong beam $E_2$ ($\omega_2$, $\mathbf{k}_2$, $\Omega_2$, vertical polarization) establishes the coherence between levels $|2\rangle$ and $|1\rangle$ (the hyperfine state $F = 3$ of $5S_{1/2}$), as well as $|0\rangle \rightarrow |2\rangle$, but with a different frequency detuning. This double-Λ energy-level structure can emit a phase-matched four-wave mixing (FWM) signal $E_F$ ($\omega_F$, $\mathbf{k}_F$, $\Omega_F$) and simultaneously provides gain for $E_1$ via optical parametric amplification with the PMC ($2\mathbf{k}_2 = \mathbf{k}_F + \mathbf{k}_1$)[39,40] shown in the dashed box in Figure 1a. The frequency detuning $\Delta_i$ is defined as the difference between the frequency $\omega_i$ and frequency interval between the two energy levels coupled by $E_i$. The other probe beam $E_1'$ ($\omega_1$, $\Omega_1$, horizontal polarization) is injected into the atomic medium along the opposite direction of $E_1$. To eliminate the potential measurement error, the corresponding

transmitted spectra are received by two branches of a balanced homodyne detector, respectively.

With the detuning $\Delta_1$ set to be near resonant with transition $|0\rangle \rightarrow |2\rangle$ and a single probe beam selectively switched on, both probe beams (with equal power of $P_{in} = 200\,\mu W$) can suffer strong resonant absorption and the output signals exhibit the same profile of intensity, demonstrating a reciprocal transmission. However, when the pump field (with a power of $P_2 = 200$ mW) is on and its detuning is set to be $\Delta_2 = -730$ MHz ($\Delta_2' = \Delta_2 + f_{HF}$, where $f_{HF} = 3.03$ GHz is the frequency gap between states $|1\rangle$ and $|0\rangle$) corresponding to the transition $|0\rangle \rightarrow |2\rangle$ ($|1\rangle \rightarrow |2\rangle$), the co-propagating probe field is effectively amplified at $\Delta_1 = 2.3$ GHz, while the output counter-propagating $E_1'$ remains to exhibit resonant absorption due to the absence of PMC. Figure 1c,d shows the output spectra of the probe beams versus the detuning $\Delta_1$ with the presence of three beams, showing that a nonreciprocal optical system is effectively achieved. In general, there should exist peaks caused by saturated absorption on the transmitted spectrum when both probe beams are present. Due to the strong absorption nature under the condition of large atomic density, nevertheless, there is no saturated absorption peak detected on the output spectra of both weak probe beams. As a result, the observed transmission spectra are the same for the situations of injecting both probe beams together or only one probe beam at a time under the condition of $P_{in} = 200\,\mu W$. A saturated absorption peak can be observed for a larger probe power [see Figure 3c].

During the generation of this parametrically amplified FWM with the interactions of the two copropagating beams, two pump photons are converted into a probe photon and a conjugate (FWM) photon simultaneously, which are viewed as a pair of twin photons. In details, the pump beam excites a spontaneous parametric (SP) FWM process with coupled Stokes (S) and anti-Stokes (aS) channels, and then the probe field is injected into corresponding channel to produce the parametrical amplification. The interaction Hamiltonian for the SPFWM process is $\hat{H} = i\hbar\kappa a_2^2 \hat{a}_S^+ \hat{a}_{aS}^+ +$ h.c., where the pumping parameter $\kappa = |-i\mu_{20}\omega_1^2 E_2^2 \chi^{(3)}/2k_1|$[41] depends on coefficient $\chi^{(3)}$ and the electric-field intensity $E_2$ of the pump beam with $\mu_{ij}$ being the dipole moment for transition $|i\rangle \rightarrow |j\rangle$. Term $a_i$ ($i = 2, S, aS$) is the creation operators corresponding to associated beams and h.c. is the Hermitian conjugate. Here the nonlinear susceptibility tensor is expressed as $\chi^{(3)} = (N\mu_{20}^2\mu_{21}^2\rho_F^{(3)})/(\varepsilon_0\hbar^3 E_2^2\Omega_F)$, in which $N$ is the atomic density, $\epsilon_0$ is the permittivity of vacuum, and density matrix element of FWM is $\rho_F^{(3)} = -i\Omega_2^2\Omega_1/\{(i\Delta_2 + \Gamma_{20})[i(\Delta_2 - \Delta_1) + \Gamma_{10}][i(2\Delta_2 - \Delta_1 + f_{HF}) + \Gamma_{10}]\}$ by solving the equations of motion under the steady-state condition via perturbation theory,[42–44] with $\Gamma_{20}$ ($\Gamma_{10}$) defined as the decay rate of $|2\rangle \rightarrow |0\rangle$ ($|1\rangle \rightarrow |0\rangle$).

With the probe field injected into the anti-Stokes channel and the vacuum field into the Stokes channel, the corresponding input-output relations can be described by the transformations of the operators $\hat{a}_S$ (FWM channel) and $\hat{a}_{aS}^+$ (probe channel)[45] as

$$\hat{a}_S \rightarrow \hat{a}_S\sqrt{G} - \hat{a}_{aS}^+\sqrt{G-1} \tag{1}$$

$$\hat{a}_{aS}^+ \rightarrow \hat{a}_{aS}^+\sqrt{G} - \hat{a}_S\sqrt{G-1} \tag{2}$$

In the above two equations, $G = \cosh^2(\kappa\tau)$ is the gain factor with $\tau$ being the time scale of interaction.[46] This is exactly the

optical parametric process and can serve as a phase-insensitive amplifier for the input probe field, in which the amplification is introduced by the nonlinearity arises from strong coupling between the probe and the FWM fields boosted by the coherence established between the hyperfine levels of the ground state.[38] For a given probe field with power $P_{in}$, powers of the output probe and FWM fields are $P_1 = GP_{in}$ and $P_F = (G-1)P_{in}$, respectively.

The output of probe channel is the focus of attention in the current work, and the corresponding transmission $T_{co} = GP_{in}$ is simulated as **Figure 2**a, in which a gain peak is effectively generated at $\Delta_1 = 2.3$ GHz and $\Delta_2 = -730$ MHz. By rearranging the probe beam in the opposite direction, its transmitted intensity is obtained as $T_{cou} = \exp[-\text{Im}(N(v)\beta\rho_{20})]P_{in}$, in which $\rho_{20} = i/[\Gamma_{20} + i(\Delta_1 + \omega_1/c)]$, $\beta = 2\pi LNu_{20}^2/(\lambda_1\epsilon_0\hbar)$ with $L$ defined as the length of the sample, and $N(v) = e^{-v^2/v_p^2}/(v_p\sqrt{\pi})$ is the Maxwell–Boltzmann velocity distribution of atoms. Here $v_p = \sqrt{2k_B T/m}$ is the most probable velocity ($k_B$ is the Boltzmann constant, $T$ is the absolute temperature, and $m$ is the atomic mass), and $v$ is the velocity that an atom moves towards the laser beams. The corresponding simulation is shown in Figure 2b, which exhibits the Doppler absorption but with a saturated absorption peak. The simulated results show the nonreciprocal propagation feature of the system.

The physical mechanism behind the emergence of the nonreciprocity can be attributed to whether the PMC being effectively realized or not. The efficiency of optical parametric amplification is greatly influenced by the parameters determining the PMC, especially the frequencies of the probe and pump beams and the angle between them. The most efficient gain occurs when the PMC is strictly satisfied with proper settings including the arrangement of a very small angle and desired laser frequencies.[41] As a consequence, compared to the counter-propagating situation with an angle of nearly 180°, the PMC in the copropagating operation can be met much better and result in a considerable gain. In the meanwhile, thermal atomic motion induces Doppler shifts for the involved laser beams, and frequency detuning $\Delta_1$ and $\Delta_2$ should be $\Delta_{1D} = \Delta_1 \pm k_1 v$ and $\Delta_{2D} = \Delta_2 + k_2 v$, respectively, where $k_1 = 2\pi/\lambda_1$ ($k_2 = 2\pi/\lambda_2$) is the wavenumber of the probe (pump) field. Therefore, the Doppler shifts for the probe and pump fields are almost the same in the copropagation case[47] considering the very small difference in wavenumbers ($\lambda_1 \approx \lambda_2$), and the two-photon resonance $\Delta_{2D} - \Delta_{1D} + f_{HF} = (\Delta_2 + k_2 v) - (\Delta_1 + k_1 v) \approx \Delta_2 - \Delta_1 + f_{HF} = 0$ (guarantees the energy conservation in PMC) for parametric gain is satisfied to excite an FWM process with a microscopic phase mismatch. This is essentially the first-order Doppler-free configuration.[47] For the counter-propagating arrangement, however, the frequency difference between the probe ($\Delta_{1D}' = \Delta_1 - k_1 v$) and pump fields "seen" by the medium becomes $\Delta_{2D} - \Delta_{1D}' + f_{HF} = \Delta_2 - \Delta_1 + 2k_1 v + f_{HF}$, which not only enlarges the phase mismatch but also destroys the required two-photon resonant condition under the same laser parameters as the copropagation case.

Figure 2c,d theoretically depict the respective nonreciprocal contrast (switching one probe beam on selectively) and corresponding isolation ratio (with both probe beams on at the same time) between the co- and counter-propagating transmissions versus the pump power $P_2$ and detuning $\Delta_2$ at $\Delta_2' - \Delta_1 = 0$. Here the nonreciprocal contrast is defined as $(T_{co} - T_{cou})/(T_{co} + T_{cou})$
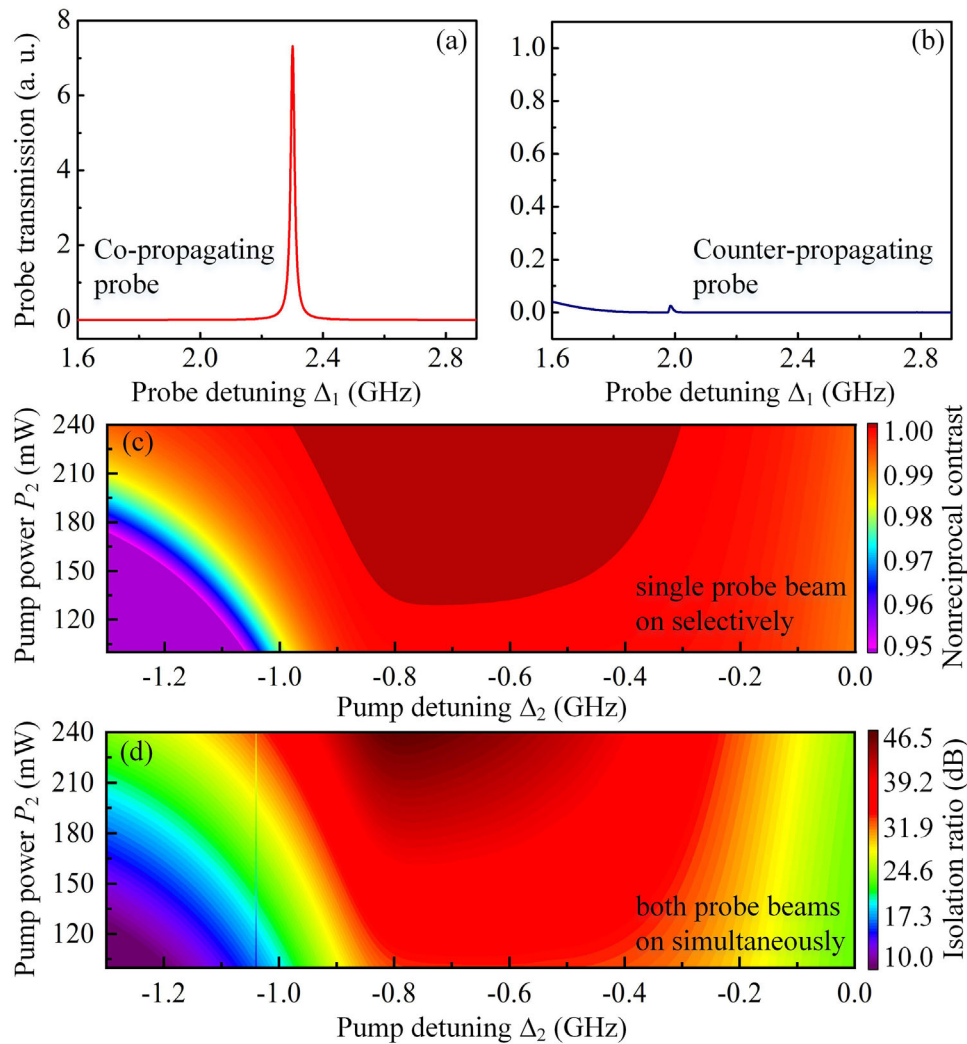
**Figure 2.** Theoretical model. Simulated output spectra of the a) co- and b) counter-propagating probe fields with both probe beams ($P_{in}$ = 650 µW) switched on at $\Delta_2$ = −730 MHz. The peak at $\Delta_1$ = 2.3 GHz on the copropagating transmission marks the center of the parametric gain, while the peak at $\Delta_1$ = 1.99 GHz on the counter-propagating transmission is caused by the saturated absorption. The simulated c) nonreciprocal contrast with only a single probe beam switched on at a time and d) isolation ratio with both probe beams on with $\Delta_2' - \Delta_1 = 0$.

and isolation ratio as $10\log_{10}(T_{co}/T_{cou})$ with $T_{co}$ ($T_{cou}$) representing the transmitted intensity of $\boldsymbol{E}_1$ ($\boldsymbol{E}_1'$) under corresponding experimental arrangement. One can see clearly that optical nonreciprocal behavior possesses a high nonreciprocal contrast ≥0.999 and gives rise to desirable isolation functionality with a large ratio ≥30 dB within a wide range of $P_2$ and $\Delta_2$. Particularly, increasing the intensity of the pump field can effectively expand the 30 dB bandwidth of optical isolation. In the current work, the 30 dB bandwidth refers to the frequency range with the isolation ratio exceeding 30 dB.

## 3. Results

**Figure 3**a demonstrates the nonreciprocal contrast by varying the power of probe beams with other parameters fixed and the corresponding isolation ratio is given in Figure 3b. The circles and curves represent respective experimental observations and relevant simulations. With the power $P_{in}$ increased from 50 to 650

µW, the measured isolation ratio changes dramatically from 26 to 43.2 dB along with the nonreciprocal contrast growing from 0.9970 to 0.9999. According to the generating principle that the parametric gain is proportional to $P_{in}$ with an amplification factor of $G$, it is readily accessible that the output intensity $T_{co}$ can be linearly enlarged with raising the incident power.

As to the counter-propagating case, the absorption coefficient experienced by the probe beam remains large due to the unchanged atomic density and laser detunings controlling the imaginary part of the susceptibility. It is easily to deduce that the output of $\boldsymbol{E}_1'$ depending on $T_{cou}$ can increase with the input $P_{in}$. However, the relatively large density of the atomic medium makes very strong absorption with the transmission approaching to (but slightly above) 0 in a wide range of the probe detuning $\Delta_1$. Increasing the input can gradually narrow the region of strong absorption, as demonstrated in Figure 3c, in which the nearly 0 transmission appears at 1.5 GHz ≤ $\Delta_1$ ≤ 3.4 GHz for the weakest $P_{in}$ = 50 µW and at 2 GHz ≤ $\Delta_1$ ≤ 3.2 GHz for the
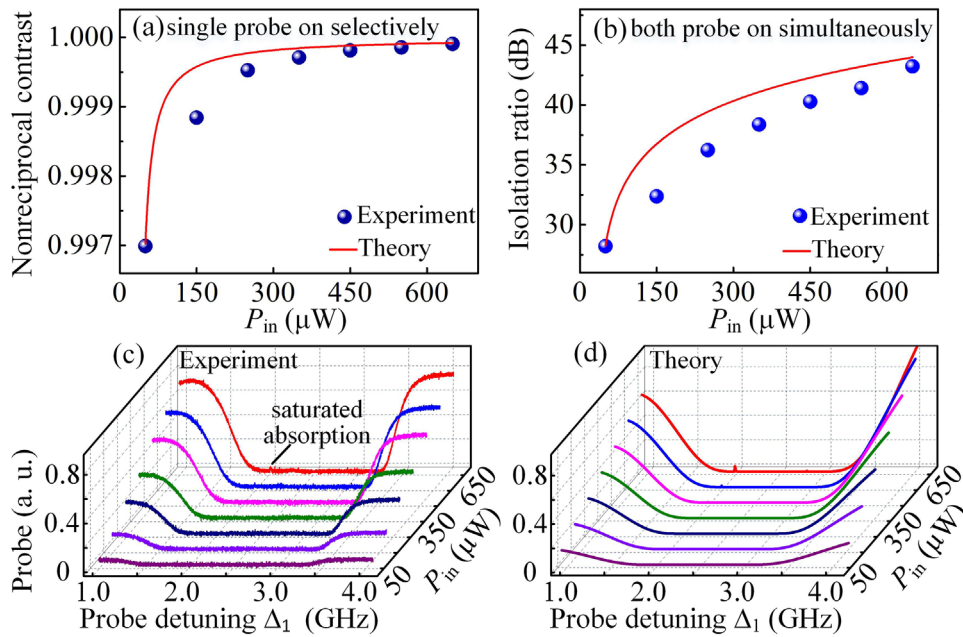
**Figure 3.** Dependence of a) nonreciprocal contrast and b) isolation ratio on the input power $P_{in}$. The incident co- and counter-propagating probe beams possess the same $P_{in}$. The detunings are $\Delta_1 = 2.3$ GHz and $\Delta_2 = -730$ MHz. The pump power is set as $P_2 = 220$ mW. The circles are experimental measurements and solid curves are corresponding calculations. The parameters of laser beams for simulation are same as the experiment. (c) and (d) show the detected and simulated spectra of the counter-propagating probe beam versus the probe detuning at different probe powers.

strongest $P_{in} = 650$ μW. Figure 3d theoretically shows the evolutions of the output intensity of counter-propagating probe beam at different $P_{in}$ and supports the observations. Considering that the parametric gain occurs at $\Delta_1 = 2.3$ GHz, the resulted $T_{co}$ can behave with a fast rising trend while $T_{cou}$ keeps unchanged near 0 within the current operating range of incident $P_{in}$, and the small peak around $\Delta_1 = 1.99$ GHz caused by the saturated absorption for $P_{in} \geq 550$ μW will impose no obvious influence on the isolation performance. In consequence, the observed nonreciprocal contrast and the isolation ratio increase with the input power, in consistence with the theoretical calculations. The results indicate that high-performance optical nonreciprocal system has been achieved for a certain range of probe power.

In addition, for a practical system involving coherently prepared atomic vapor, noises may be introduced through the fluctuations of laser power and atomic temperature, as well as electrical noise from the photoelectric detector. The power fluctuation of the output from an external-cavity diode laser is typically less than ±0.5%, which leads a variation of less than ±0.07 dB on the isolation ratio. The long-term stability of the atomic temperature is ±0.01 °C, which can result in the variation of atomic density $N$ with a ratio of ≈±0.06% as well as the fluctuation of the isolation ratio in the range of ±0.02 dB. The change of isolation ratio caused by the fluctuation of systemic parameters is much smaller than the measurements. Also, during the calculation of isolation ratio, the electrical background offset (measured with both probe beams blocked) of the photoelectric detector is removed. Namely, $T_{co}$ ($T_{cou}$) is obtained by taken the difference between the measured transmitted intensity of the copropagating (counter-propagating) probe and average background offset.

Furthermore, we investigate the evolutions of the transmission contrast and isolation ratio versus the intensity and detuning of

the pump beam that can significantly modify the efficiency of the parametric amplification but have little influence on the counter-propagating probe field. As shown in **Figure 4**a,b, both the nonreciprocal transmission and isolation performance are improved under the condition of stronger pump intensity. Remarkably, the experimental isolation ratio is enhanced from to 33 to 45.8 dB when power $P_2$ of the pump field increases from 100 to 240 mW with the input power set as $P_{in} = 650$ μW. According to the simulated plot given by the solid curve, the isolation ration can deserve further improvement for a higher pump power. However, subject to the upper limit of output from our semiconductor tapered laser amplifier, we can provide a maximum $P_2 = 240$ mW at present.

Figure 4c reveals the measured isolation bandwidth by discretely manipulating the pump detuning with pump power $P_2 = 240$ mW. The isolation ratio changes considerably within the detuning $\Delta_2$ ranging from −1.2 to −0.1 GHz. The maximum isolation ratio of 46.5 dB appears at $\Delta_2 = -0.85$ GHz. The 30 dB bandwidth of isolation ratio reaches 0.85 GHz. The abrupt decline of the isolation ratio around $\Delta_2 = -1.04$ GHz (the minimum isolation ratio is about 28.4 dB) on the simulated curve is due to the presence of the saturated absorption peak, which increases $T_{cou}$. The region with the isolation ratio < 30 dB is less than 1 MHz and exerts little influence on the 30 dB bandwidth.

## 4. Summary

In summary, we have experimentally demonstrated that the optical parametric amplification in a coherently prepared atomic system can provide an effective route to realize desirable optical isolation with both high isolation ratio and broad bandwidth. Compared to the existing cavity-free nonreciprocal studies with high isolation ratio based on atomic coherence, our scheme is
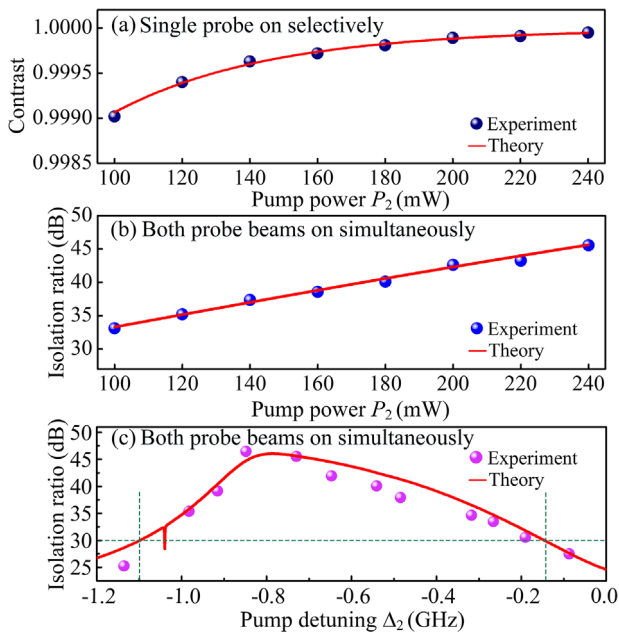
**Figure 4.** Evolution of the nonreciprocal and isolation performance versus pump-field parameters. a) Transmission contrast and b) isolation ratio versus the pump power $P_2$ with a fixed input of $P_{in} = 650\ \mu W$ (for both input probe beams). The experimental observations and calculations are marked by circles and solid curves, respectively. The parameters for the simulations are the same as those in Figure 3. c) The measured isolation ratio at different pump-field detuning $\Delta_2$.

performed in a three-level system requiring only one pump field, rather than a four-level configuration with two additional driving fields,[19,21] and is easier for potential miniaturization and system integration considering the development of chip-scale-integrated vapor cells.[48] Therefore, the achieved optical nonreciprocal behavior arising from satisfying the degree of PMC for optical parametric process can undoubtedly pave a practical and simple way to optimize and explore nonreciprocity-based optical functionalities. Moreover, the adopted double-$\Lambda$ atomic system can be employed to simultaneously produce entangled photon pairs and squeezing states, indicating that the optical nonreciprocity born with quantum nature may open a new door to design nonreciprocal quantum devices.

## Acknowledgements

## Conflict of Interest

The authors declare no conflict of interest.

## Data Availability Statement

The data that support the findings of this study are available from the corresponding author upon reasonable request.

[1] D. Jalas, A. Petrov, M. Eich, W. Freude, S. Fan, Z. Yu, R. Baets, M. Popović, A. Melloni, J. D. Joannopoulos, M. Vanwolleghem, C. R. Doerr, H. Renner, *Nat. Photonics* **2013**, *7*, 579.

[2] P. Lodahl, S. Mahmoodian, S. Stobbe, A. Rauschenbeutel, P. Schneewiss, J. Volz, H. Pichler, P. Zoller, *Nature* **2017**, *541*, 473.

[3] Z. Yu, S. Fan, *Nat. Photonics* **2009**, *3*, 91.

[4] N. A. Estep, D. L. Sounas, J. Soric, A. Alù, *Nat. Phys.* **2014**, *10*, 923.

[5] T. T. Koutserimpas, R. Fleury, *Phys. Rev. Lett.* **2018**, *120*, 087401.

[6] A. B. Khanikaev, A. Alù, *Nat. Photonics* **2015**, *9*, 359.

[7] Y. Shi, Z. F. Yu, S. H. Fan, *Nat. Photonics* **2015**, *9*, 388.

[8] L. Chang, X. Jiang, S. Hua, C. Yang, J. Wen, L. Jiang, G. Li, G. Wang, M. Xiao, *Nat. Photonics* **2014**, *8*, 524.

[9] K. Xia, F. Nori, M. Xiao, *Phys. Rev. Lett.* **2018**, *121*, 203602.

[10] H. Tian, J. Liu, A. Siddharth, R. N. Wang, T. Blésin, J. He, T. J. Kippenberg, S. A. Bhave, *Nat. Photonics* **2021**, *15*, 828.

[11] D. B. Sohn, O. E. Örsel, G. Bahl, *Nat. Photonics* **2021**, *15*, 822.

[12] X. Huang, C. Lu, C. Liang, H. Tao, Y. Liu, *Light: Sci. Appl.* **2021**, *10*, 30.

[13] L. Bi, J. Hu, P. Jiang, D. H. Kim, G. F. Dionne, L. C. Kimerling, C. A. Ross, *Nat. Photonics* **2011**, *5*, 758.

[14] M. Scheucher, A. Hilico, E. Will, J. Volz, A. Rauschenbeutel, *Science* **2016**, *354*, 1577.

[15] Z. Shen, Y.-L. Zhang, Y. Chen, F.-W. Sun, X.-B. Zou, G.-C. Guo, C.-L. Zou, C.-H. Dong, *Nat. Commun.* **2018**, *9*, 1797.

[16] L. D. Bino, J. M. Silver, M. T. M. Woodley, S. L. Stebbings, X. Zhao, P. DelHaye, *Optica* **2018**, *5*, 279.

[17] I. Söllner, S. Mahmoodian, S. L. Hansen, L. Midolo, A. Javadi, G. Kirŝanske, T. Pregnolato, H. El-Ella, E. H. Lee, J. D. Song, S. Stobbe, P. Lodahl, *Nat. Nanotechnol.* **2015**, *10*, 775.

[18] S. Zhang, Y. Hu, G. Lin, Y. Niu, K. Xia, J. Gong, S. Gong, *Nat. Photonics* **2018**, *12*, 744.

[19] G. Lin, S. Zhang, Y. Hu, Y. Niu, J. Gong, S. Gong, *Phys. Rev. Lett.* **2019**, *123*, 033902.

[20] M. Dong, K. Xia, W. Zhang, Y. Yu, Y. Ye, E. Li, L. Zeng, D. Ding, B. Shi, G. Guo, F. Nori, *Sci. Adv.* **2021**, *7*, eabe8924.

[21] C. Liang, B. Liu, A. Xu, X. Wen, C. Lu, K. Xia, M. K. Tey, Y. Liu, L. You, *Phys. Rev. Lett.* **2020**, *125*, 123901.

[22] P. Yang, X. Xia, H. He, S. Li, X. Han, P. Zhang, G. Li, P. Zhang, J. Xu, Y. Yang, T. Zhang, *Phys. Rev. Lett.* **2019**, *123*, 233604.

[23] F. Song, Z. Wang, E. Li, Z. Huang, B. Yu, B. Shi, *Appl. Phys. Lett.* **2021**, *119*, 024101.

[24] X. Lu, W. Cao, W. Yi, H. Shen, Y. Xiao, *Phys. Rev. Lett.* **2021**, *126*, 223603.

[25] S. A. R. Horsley, J. Wu, M. Artoni, G. C. La Rocca, *Phys. Rev. Lett.* **2013**, *110*, 223602.

[26] A. Mekawy, D. L. Sounas, A. Alù, *Photonics* **2021**, *8*, 139.

[27] R. Ritter, N. Gruhler, H. Dobbertin, H. Kübler, S. Scheel, W. Pernice, T. Pfau, R. Löw, *Phys. Rev. X* **2018**, *8*, 021032.

[28] P. Londero, V. Venkataraman, A. R. Bhagwat, A. D. Slepkov, A. L. Gaeta, *Phys. Rev. Lett.* **2009**, *103*, 043602.

[29] X. Hu, Z. Wang, P. Zhang, G. Chen, Y. Zhang, G. Li, X. Zou, T. Zhang, Hong X. Tang, C. Dong, G. Guo, C. Zou, *Nat. Commun.* **2021**, *12*, 2389.

[30] D. Malz, L. D. Tóth, N. R. Bernier, A. K. Feofanov, T. J. Kippenberg, A. Nunnenkamp, *Phys. Rev. Lett.* **2018**, *120*, 023601.

**ADVANCED
SCIENCE NEWS**

www.advancedsciencenews.com

**LASER
& PHOTONICS
REVIEWS**

www.lpr-journal.org

[31] S. Buddhiraju, A. Song, G. T. Papadakis, S. Fan, *Phys. Rev. Lett.* **2020**, *124*, 257403.

[32] B. Peng, Ş. Kaya Özdemir, F. Lei, F. Monifi, M. Gianfreda, G. Long, S. Fan, F. Nori, C. M. Bender, L. Yang, *Nat. Phys.* **2014**, *10*, 394.

[33] N. T. Otterstrom, E. A. Kittlaus, S. Gertler, R. O. Behunin, A. L. Lentine, P. T. Rakich, *Optica* **2019**, *6*, 1117.

[34] M. Lawrence, J. A. Dionne, *Nat. Commun.* **2019**, *10*, 3297.

[35] K. Fang, J. Luo, A. Metelmann, M. H. Matheny, F. Marquardt, A. A. Clerk, O. Painter, *Nat. Phys.* **2017**, *13*, 465.

[36] S. Hua, J. Wen, X. Jiang, Q. Hua, L. Jiang, M. Xiao, *Nat. Commun.* **2016**, *7*, 13657.

[37] Y. X. Chen, S. S. Liu, Y. B. Lou, J. T. Jing, *Phys. Rev. Lett.* **2021**, *127*, 093601.

[38] R. C. Pooser, A. M. Marino, V. Boyer, K. M. Jones, P. D. Lett, *Phys. Rev. Lett.* **2009**, *103*, 010501.

[39] V. Boyer, A. M. Marino, R. C. Pooser, P. D. Lett, *Science* **2008**, *321*, 544.

[40] X. Pan, S. Yu, Y. Zhou, K. Zhang, K. Zhang, S. Lv, S. Li, W. Wang, J. Jing, *Phys. Rev. Lett.* **2019**, *123*, 070506.

[41] M. T. Turnbull, P. G. Petrov, C. S. Embrey, A. M. Marino, V. Boyer, *Phys. Rev. A* **2013**, *88*, 033845.

[42] J. M. Wen, M. H. Rubin, *Phys. Rev. A* **2006**, *74*, 023808.

[43] Y. P. Zhang, A. W. Brown, M. Xiao, *Phys. Rev. Lett.* **2007**, *99*, 123603.

[44] Z. C. Zuo, J. Sun, X. Liu, Q. Jiang, G. S. Fu, L. A. Wu, P. M. Fu, *Phys. Rev. Lett.* **2006**, *97*, 193904.

[45] C. F. McCormick, A. M. Marino, V. Boyer, P. D. Lett, *Phys. Rev. A* **2008**, *78*, 043816.

[46] S. Liu, Y. Lou, J. Jing, *Nat. Commun.* **2020**, *11*, 3875.

[47] J. Gea-Banacloche, Y.-q. Li, S.-z. Jin, M. Xiao, *Phys. Rev. A* **1995**, *51*, 576.

[48] R. Zektzer, N. Mazurski, Y. Barash, U. Ievy, *Nat. Photonics* **2021**, *15*, 772.